Synthesis of Monodisperse Silica Nanospheres and Titania Beads from Rotating Cylinder System

Thi Thu Hien NGUYEN [1], Sohyeon SUNG [2], Quang Hai TRAN [1], Young-Sang CHO [1]

[1] *Department of Chemical Engineering and Biotechnology, Tech University of Korea, 237 Sangidaehak-ro, Siheung-si, Gyeong-gi, 15073, Republic of Korea*
[2] *Advances Materials Division, Korea Research Institute of Chemical Technology, Daejeon 34114, Republic of Korea*

http://doi.org/10.5755/j02.ms.34423

Received 29 June 2023; accepted 24 January 2024

Economic raw materials such as low-grade ethanol and Tetraethyl Ortosilicate (TEOS) were adopted as reactants for the synthesis of monodisperse silica nanospheres using a Taylor Vortex flow reactor with a rotating cylinder system. Factors affecting the mean diameter and size distribution of the silica grains were investigated by changing the rotating speed of the inner cylinder and the composition of reactants. In the case of titania beads, grain diameter size was adjusted by changing the amount of precursor (titanium (IV) isopropoxide, TIP), hexadecylamine (HDA) or Potassium Chloride (KCl) and reaction temperature as well as the rotation speed of the cylinder. As a demonstrative application, titania beads could be used for the removal of organic dye as a model contaminant dissolved in an aqueous medium using a photocatalytic decomposition system.
Keywords: rotating cylinder system, Taylor Vortex flow reactor, monodisperse silica nanospheres, titania beads, photocatalysis, mean diameter.

1. INTRODUCTION

Synthesis of functional silica and titania grains is attracting much attention for useful applications including reflective pigment for display and photoelectrode material for solar cells [1, 2]. In laboratory-scale research, most synthesis routes have been studied by using a conventional mixing system composed of the flask and stirring paddle. However, this system may have drawbacks, since non-uniform mixing can be generated in certain parts of the reactor, causing a 'dead zone' [3]. To overcome this, rotating cylinder systems consisting of rotating inner cylinder and stationary outer cylinder has been developed for micro-scale mixing and facile rpm control [4, 5]. After the concept of the Taylor Vortex was developed, rotating cylinder systems were adopted for various engineering applications such as slurry preparation, crystallization in the food industry, and synthesis of functional materials such as graphene and energy materials [6 – 11].

Silica nanospheres with narrow size distribution have been studied intensively to apply colloidal crystals with photonic band gap properties [12]. Since artificial opals can be used for chemical or biological sensors as well as reflective pigments, many commercial routes are available to purchase such grains [13 – 15]. Until now, monodisperse silica nanospheres have been synthesized using high-purity reagent-grade chemicals as silica precursor and reaction solvent to suppress unexpected results due to impurities [16]. However, it is advantageous to use low-grade chemicals for grain formation with sufficient monodispersity in industrial applications.

In addition to silica grains, titania beads have been considered as promising material for photovoltaic applications [17]. Since such grains have been synthesized by hydrothermal reaction under harsh reaction conditions at high temperature and pressure, it is necessary to develop novel reaction route for the synthesis of such grains at room temperature and ambient pressure [18].

In this study, the rotating cylinder system (Taylor Vortex flow reactors) exhibits great advantages in synthesizing ceramic grains and was proposed to study the effects of operation conditions of the reactor on grain monodispersity and morphologies. First, monodisperse silica nanospheres were synthesized using economic raw materials like low-grade TEOS as the starting chemical material of silica. Since high-purity reagent-grade solvent or precursor materials are inadequate for industrial production of such grains, low-grade precursor is advantageous to large-scale synthesis of silica nanospheres with narrow size distribution. Second, titania beads were obtained from TIP (titanium (IV) isopropoxide) as precursor by adjusting the reaction conditions such as reaction temperature, rotation speed, and concentration of reactants for demonstrative application of photocatalytic decomposition of organic dye in an aqueous medium.

2. EXPERIMENTAL

2.1. Materials and reagents

Ethanol for washing solvent (98 %) was used as a reaction medium for silica nanospheres and purchased from Daejung Chemicals. Ammonium hydroxide was used as a catalyst for hydrolysis reaction and procured from Sigma-

* Corresponding author. Tel.: +82-3180410612.
E-mail: *yscho78@tukorea.ac.kr* (Y. S. Cho)

Aldrich. Tetraethylorthosilicate (TEOS, 99 %) was used as a silica source and bought from Sigma-Aldrich. For the synthesis of titania beads, titanium (IV) isopropoxide (TIP, ≥ 97.0 %) was used as a precursor and purchased from Sigma-Aldrich. Ethanol (HPLC, 99.9 %, Deajung Chemicals), Hexadecylamine (HDA, 90 %, Sigma-Aldrich), Potassium Chloride (KCl, Kanto Chemical Co., Inc.) was used as reaction medium and catalyst for the synthesis reaction.

2.2. Synthesis of monodisperse silica nanospheres by Taylor Vortex reactor

For the synthesis of silica nanospheres, 20 mL ethanol was poured into the reactor, followed by the addition of ammonium hydroxide, while the inner cylinder rotated from 90 to 900 rpm. Then, 0.1 mL TEOS dissolved in 4 mL ethanol was added to the reactor to produce seed grains. After 1.5 hours, 1.6 mL TEOS dissolved in 6.4 mL ethanol was added to the reactor for 1st growth step in typical experiments. If necessary, an additional amount of TEOS was added to the reactor after 2 hours of reaction for the additional growth step. The final grains were washed in fresh ethanol by repeated centrifugation and redispersion by sonication.

The Taylor Vortex flow reactor consisted of an outer cylinder (30 mm diameter, 130 mm length) and a stainless-steel inner cylinder (24 mm diameter, 130 mm length) with a common axis shown in Fig. 1 a was adopted for laboratory-scale experiments by using 33 mL actual volume.

2.3. Synthesis of titania beads by Taylor Vortex reactor and round bottom flask

TiO_2 beads were prepared via a sol-gel process in the presence of HDA as a structure-directing agent [19]. For the synthesis of titania beads, ethanol (25 mL) was mixed with HDA (0.042 g) and then poured into the reactor, followed by the addition of 0.01 mL KCl (0.033 M) and 0.01 mL TIP. The inner cylinder was rotated at adequate rpm (300 to 600 rpm). After 18 hours, the obtained products were centrifuged, rinsed with fresh ethanol three times, and dried for SEM observation. Calcination was performed using a box furnace at 450 °C for 5 hours to observe the size change of titania beads.

For comparison, TiO_2 beads were fabricated by round bottom flask (100 mL) under the same conditions.

2.4. Photocatalytic removal of methylene blue

For the photocatalytic decomposition of methylene blue, the aqueous suspension of titania beads (25 mL) was prepared at a concentration of 0.0002 g/mL after mild sonication. Separately, 25 mL of the aqueous solution of methylene blue (Daejung Chemicals & Metals Co., LTD) was arranged with 0.00002 g/mL as an initial dose, followed by mixing the suspension of titania beads. The resulting mixture was agitated under UV illumination (Blacklight blue, Sankyo Denki, 352 nm, 10 W, 8 UV lamps). The aqueous solution of methylene blue was stirred at 300 rpm with the aqueous suspension of titania beads and then put in a dark room for 30 min for equilibration between methylene blue and titania beads before the photocatalytic degradation. The first sample was obtained (C_0; t = 0) after 30 minutes in the dark. The concentration change of methylene blue was monitored at regular time intervals using UV-vis spectrophotometer. Concentrations of methylene blue were determined from the absorbance at 664 nm [20, 21] wavelength, and photocatalysis was performed for 240 minutes.

2.5. Characterizations

The morphologies of monodisperse silica nanospheres grains were observed using a field emission scanning electron microscope (FE-SEM, Hitachi-S4700). The morphologies of titania beads were characterized by field emission scanning electron microscopy (CX_200 Plus, COXEM). FT-IR spectra of the grains were measured using an FT-IR spectrometer (Nicolet iS5, Thermo Fisher Scientific Co. Ltd). The concentration of methylene blue in an aqueous solution was measured using a UV-visible spectrometer (OPTIZEN POP, Mecasys Co., Ltd). Powder X-ray diffraction of titania beads was measured using an XRD machine (D2 Phaser, Bruker).

3. RESULTS AND DISCUSSION

In this study, ceramic grains such as monodisperse silica nanospheres or titania beads were synthesized using a rotating cylinder system (Taylor Vortex flow reactor, Laminar). To investigate the effect of mixing speed, the reactor was designed to control the rotation rate of an inner cylinder at various rpms. To control the size of silica nanospheres, the seeded growth scheme was applied by successive growth of the grains by subsequent addition of reactants after the formation of seed grains, as displayed schematically in Fig. 1 b. Furthermore, titania beads were prepared via a sol-gel process in the presence of HDA as a structure-directing agent as shown in Fig. 1 c [22]. Fig. 1 c shows a schematic diagram of a possible mechanism for the beads' growth process. Titania beads are formed through a cooperative assembly process involving long-c hain alkylamine and $Ti(OCH(CH_3)_2)_{4-x}(OH)_x$ species. The resultant $Ti(OCH(CH_3)_2)_{4-x}(OH)_x$ species on hydrolysis of Titanium (IV) isopropoxide (TIP) participate in hydrogen-bonding interactions with amino groups of the Hexadecylamine (HDA) [22].

In this study, the reaction temperature of the rotating cylinder system was adjusted from room temperature to 60 °C for control of the size of monodisperse silica nanospheres. As shown in the SEM images in Fig. 2 a – c silica nanospheres with narrow size distribution could be synthesized by 1st growth of the seed grains, while the inner cylinder rotated at 900 rpm. The mean diameter could be controlled from about 200 to 600 nm, and the size reduction was observed with increasing temperature. Because the reaction rate increases with increasing temperature, the number of seed grains increases as temperature increases, causing the increase of grain number density and reduction of the size of the grown grains under the same reactant concentrations. Thus, the overall trend of decrease in grain size with increasing temperature was observed as displayed in the graph of Fig. 2 d. Since the standard deviation of silica nanospheres is another important factor for the estimation of grain monodispersity, the size distribution of

each sample was obtained by measuring the diameters of 100 grains from sn electron microscope image, and the standard deviation was measured. With increasing reaction temperature, the diameter of silica nanospheres decreased, and the standard deviation of grains increased, as shown in the inset graph of Fig. 2 d.

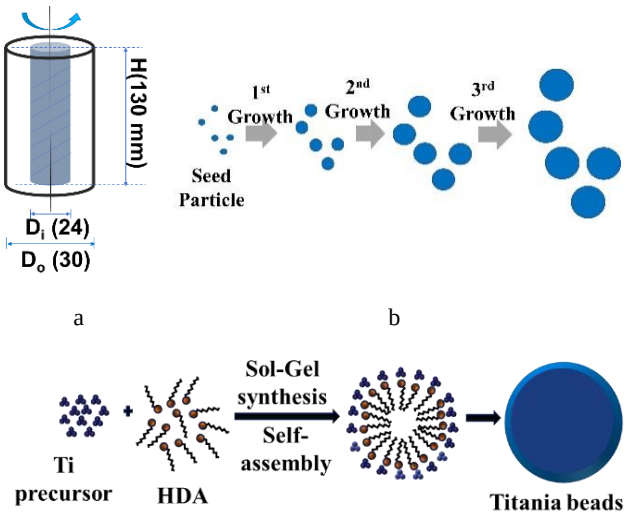

a b c

Fig. 1. a – schematic figure of rotating cylinder system; reaction during mixing by rotation of the inner cylinder can be carried out inside the annulus region of the concentric system; b – synthesis process of monodisperse silica nanospheres by seeded growth method; c – the synthesis process of titania beads using a rotating cylinder system

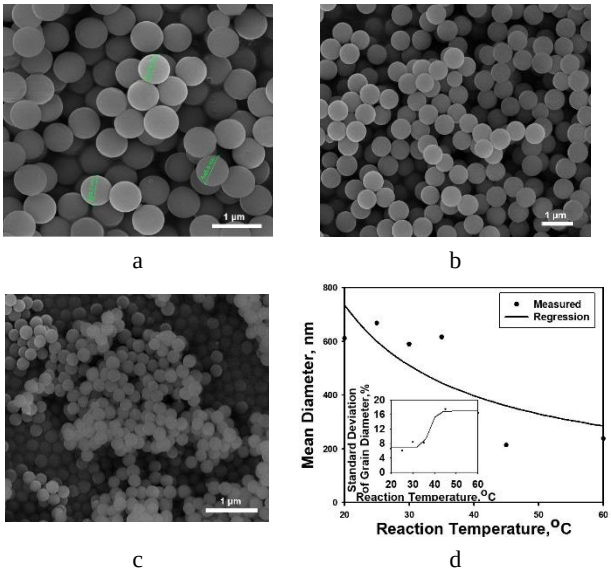

a b c d

Fig. 2. SEM image of silica nanospheres synthesized from rotating cylinder system at: a – 20 °C; b – 35 °C; c – 60 °C; d – change of mean diameter and standard deviation of the silica nanospheres as a function of reaction temperature. The grains were synthesized from the seed grains, followed by the 1st growth. The rotation speed of the inner cylinder was maintained at 900 rpm

In addition to reaction temperature, the effect of catalyst concentration on grain size of silica nanospheres was investigated by changing the amount of ammonium hydroxide, while reaction temperature and rotation speed were maintained at 35 °C and 900 rpm, respectively until the 1st growth of the grains. When theamount of ammonia was too small, bimodal size distribution was obtained, as shown in the SEM image of Fig. 3 a, and size distribution in a graph of Fig. 3 b. Because the amount of catalyst for hydrolysis and condensation of raw material, TEOS, became insufficient at low ammonia concentration, further growth of some seed grains became difficult, causing bimodal distribution of silica nanospheres. However, monodisperse silica nanospheres with 637.7 nm in diameter could be synthesized, when the amount of ammonia increased to 4 mL, implying that the optimum amount of the catalyst can be confirmed from the grains morphologies shown in the SEM image in Fig. 2 b. Although the further increase of ammonia (5 mL) also resulted in the synthesis of monomodal silica nanospheres with similar grain diameter, 575.7 nm shown in the SEM image of Fig. 3 c, the standard deviation of the grains increased, causing slightly broader size distribution of the grains. Because concentrated ammonia solution may increase the reaction rate of hydrolysis and condensation of TEOS, a faster mixing rate may be necessary to obtain monomodal grains with a more uniform size distribution.

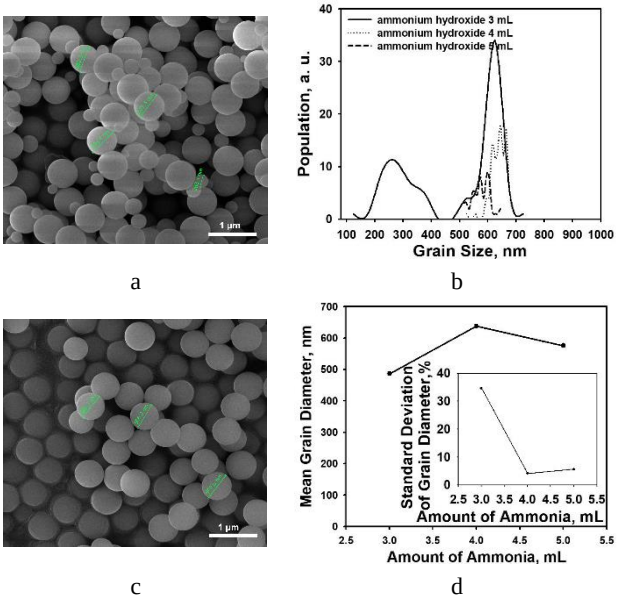

a b c d

Fig. 3. a – SEM image of silica nanospheres synthesized from a rotating cylinder system using 3 mL of ammonium hydroxide solution at 35 °C; b – size distribution of silica nanospheres synthesized using various amount of ammonium hydroxide; c – SEM image of silica nanospheres synthesized from a rotating cylinder system using 5 mL of ammonium hydroxide solution at 35 °C; d – change of mean diameter and standard deviation of the silica nanospheres as a function of the amount of ammonium hydroxide solution. The grains were synthesized from the seed grains, followed by the 1st growth. The rotation speed of the inner cylinder was maintained at 900 rpm

In this study, the effect of precursor concentration on grain monodispersity was also studied by changing the amount of TEOS. While reaction temperature and mixing speed were maintained at 35 °C and 900 rpm, respectively until 1st growth, the amount of ammonia was fixed at 5 mL Although the resulting grain morphologies were spherical as

shown in SEM images of Fig. 4 a – b, the variation of the grain size as a function of the amount of TEOS was relatively small, as displayed in the graph of Fig. 4 c. However, anexcess amount of TEOS resulted in the formation of silica nanospheres with broad size distribution and larger value of standard deviation, as shown in the inset graph of Fig. 4 c. Since an excess amount of precursor causes the formation of small new grains during the 1st growth step of the seed grains, the resulting silica nanospheres can be polydisperse, as shown in the SEM image of Fig. 4 b.

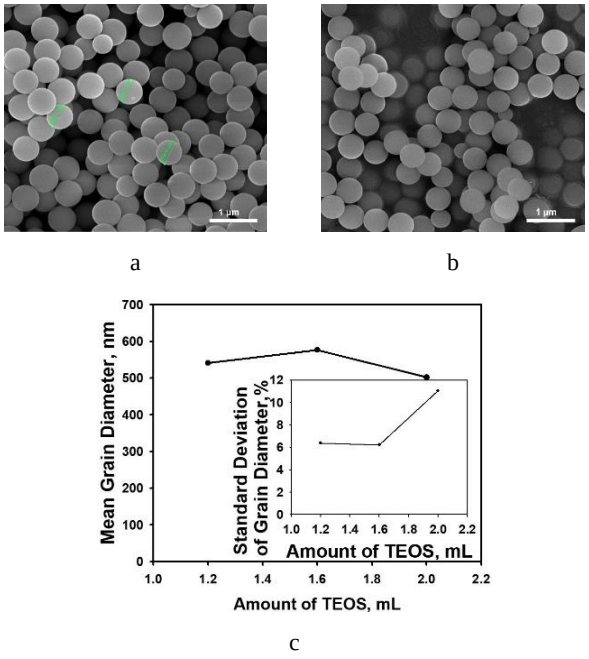

Fig. 4. SEM image of silica nanospheres synthesized from a rotating cylinder system using: a – 1.2 mL; b – 2 mL of TEOS at 35 °C; c – change of mean diameter and standard deviation of the silica nanospheres as a function of the amount of TEOS. The grains were synthesized from the seed grains, followed by the 1st growth. The amount of ammonia was fixed as 5 mL. The rotation speed of the inner cylinder was maintained at 900 rpm

The advantage of a rotating cylinder system as a chemical reactor is that facile control of the mixing rate is possible by adjusting the rotation speed of the inner cylinder. In this study, the effect of mixing rate on the grain monodispersity of silica nanospheres was studied by changing the mixing rate from 90 to 900 rpm, while the amount of ammonia and reaction temperature were maintained at 4 mL and 35 °C. When the rotation speed was too slow, bimodal grains were obtained as shown in the SEM images of Fig. 5 a, b. Since it is difficult to expect the complete mixing of reactants and seed grains at low mixing speed, further growth of some seed grains cannot be guaranteed, causing small seed and bigger grown grains. However, 505 rpm was fast enough to form monodisperse silica nanospheres with 675.7 nm as the average diameter and 43.5 nm as the standard deviation, as displayed in the SEM image of Fig. 5 c. When mixing rate increased to 900 rpm, similar monodispersity could be obtained, as shown in the inset graph of Fig. 5 d. In addition to the standard deviation of the grains, the average diameter was also affected by the rotating speed of the inner cylinder, as shown in the graph of Fig. 5 d. When the mixing rate became faster, the average size of silica nanospheres increased, and grain size was rarely affected by the further increase in mixing rate. This can be interpreted by shear-induced flocculation, causing the formation of larger grains during the synthesis of slurries or suspensions [23, 24].

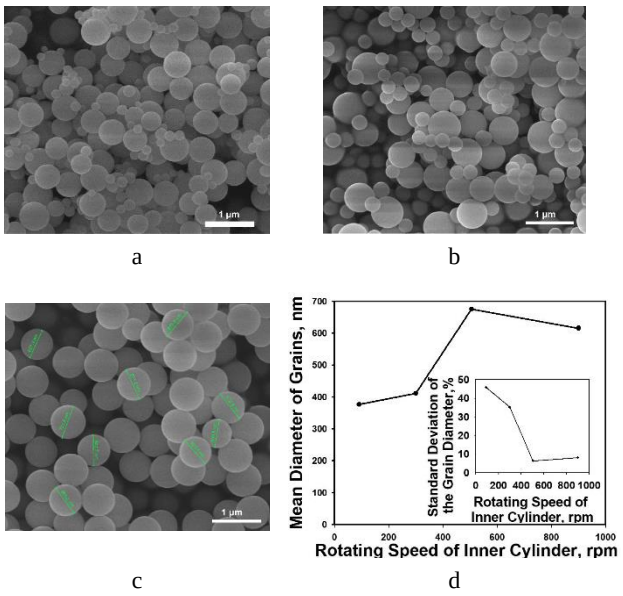

Fig. 5. SEM image of silica nanospheres synthesized from rotating cylinder system at: a – 90 rpm; b – 300 rpm; c – 505 rpm; d – change of mean diameter and standard deviation of the silica nanospheres as a function of the rotating speed of the inner cylinder. The grains were synthesized from the seed grains, followed by the 1st growth. The amount of ammonia and reaction temperature were maintained at 4 mL and 35 °C

Because it is difficult to synthesize large grains by the 1st growth, additional growth steps were also tried to prepare uniform silica nanospheres with increased diameter. As shown in the SEM image of Fig. 6 a, the average diameter of the silica nanospheres increased to about 670 nm from 616 nm after the 2nd growth step at 35 °C and 900 rpm. Though the results are not reproduced here, average size of seed grains before the 1st growth was measured as 140 nm with 23.5 nm as standard deviation. After 3rd growth, average grain size increased to 770 nm, as shown in SEM image of Fig. 6 b. Because secondary nuclei can be produced during each growth step, the size distribution of silica nanospheres became more broader as the growth step increased, as displayed in the graph of Fig. 6 c. The chemical characteristic of the silica grains was confirmed from FT-IR spectrum in Fig. 6 d, indicating that amorphous silica could be obtained after the reaction, since characteristic peaks were observed from 1057, 952 and 795 cm^{-1}. The two vibrations in the range 1057 and 952 cm^{-1} are assignable to Si-O-Si and Si-O vibration modes of isolated Si-OH groups, respectively [25 – 27]. The peak at 795 cm^{-1} is assignable to the O-Si-O vibration mode of SiO_2 [25]. The IR spectrum of SiO_2, thus demonstrates the presence of all the vibrational bands of Si-OH, O-Si-O and Si-O-Si typical of amorphous SiO_2.

After the synthesis of silica nanospheres using a rotating cylinder system, the synthesis of titania beads was studied from the Taylor vortex reactor.

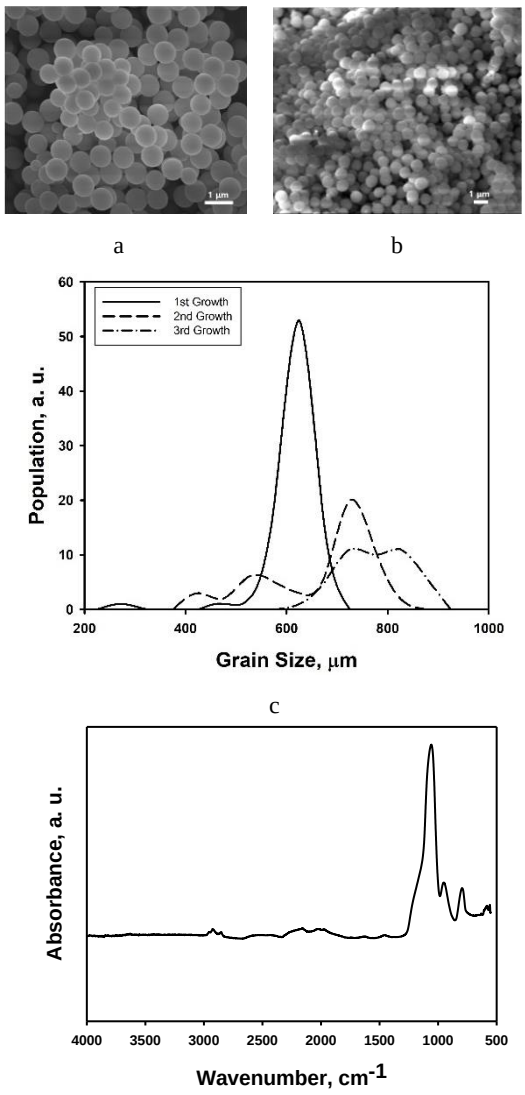

Fig. 6. SEM image of silica nanospheres synthesized by seeded growth method after: a – 2nd; b – 3rd growth from rotating cylinder system at 900 rpm; c – size distribution of monodisperse silica nanospheres after the 1st, 2nd, and 3rd growth. Reaction temperature was maintained at 35 °C; d – FT-IR spectra of silica grains synthesized using a rotating cylinder system

In this study, the effect of mixing rate was investigated by changing the rotation speed from 200 to 600 rpm, while the reaction performed at room temperature, the amount of KCl (0.033 M), TIP, and HDA were maintained as 0.1 mL, 0.1 mL, and 0.042 g, respectively, and results shown as SEM images in Fig. 7 a – e. When rotation speed became faster from 300 to 375 rpm, the mean diameter of titania beads increased. From 450 to 600 rpm, the mean diameter of titania beads does not change much, as displayed in the graph of Fig. 7 f, and the standard deviation of grains was also analyzed, as shown in the inset graph of Fig. 7 f. That was similar to the above synthesis of silica monodisperse nanograins, which, due to shear-induced flocculation, form larger grains during synthesis.

In this study, the reaction temperature of the rotating cylinder system was adjusted from 25 to 55 °C for control of the size of titania beads.

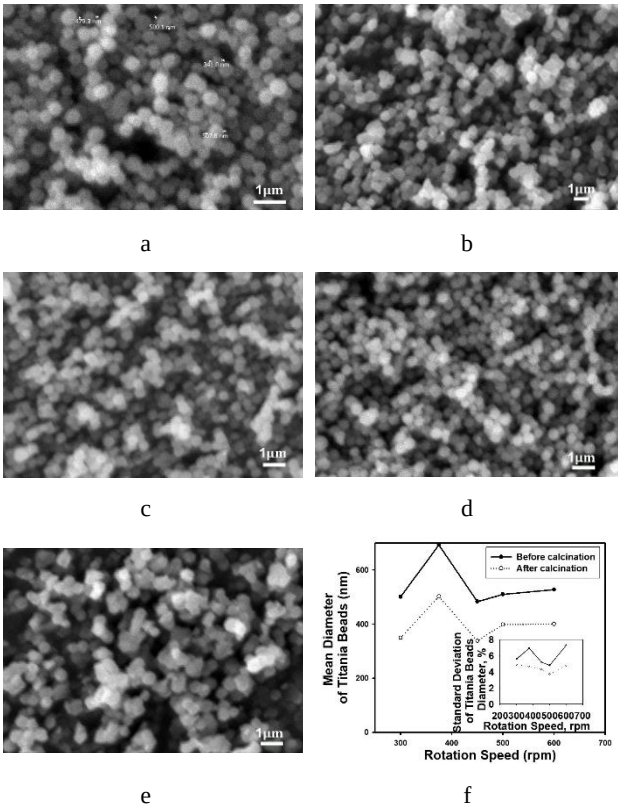

Fig. 7. SEM image of titania beads before calcination synthesized using 0.042 g HDA, 0.1 mL TIP, 0.1 mL KCl (0.033 M) at: a – 300 rpm; b – 375 rpm; c – 450 rpm; d – 500 rpm; e – 600 rpm; f – change of mean diameter and standard deviation of the titania beads as a function of the rotating speed of the inner cylinder. The temperature of the rotating cylinder system was maintained at room temperature

As shown in the SEM images in Fig. 8 a – d, titania beads with narrow size distribution could be synthesized, while the inner cylinder rotated at 300 rpm. Before calcination for 450 °C in 5 hours, the mean diameter could be controlled from about 600.88 to 515.47 nm, after calcination mean diameter could be controlled from 468.51 to 378.88 nm, and the size reduction was observed with increasing temperature was observed as displayed in the graph of Fig. 8 e. Similar to the fabrication principle of the above silica grain, when temperature increased, the reaction rate increased, causing the increase of grain number density and reducing the size of the titania beads under the same reactant concentrations. And size distribution of each sample was obtained by measuring the diameter of a few titania beads, and the standard deviation was measured. With increasing reaction temperature, the diameter of titania beads decreased, and the standard deviation of grains increased, as shown in the inset graph of Fig. 8 e.

In addition to reaction temperature and rotation speed, the effect of catalyst concentration on the grain size of titania beads was investigated by changing the amount of TIP, HDA, and KCl, while reacting at room temperature and 300 rpm of rotation speed. First, the effect of precursor concentration was studied by changing TIP and HDA by the same amount. For example, if the amount of TIP is reduced by 2 times, the amount of HDA is also reduced by 2 times, while reaction temperature and mixing speed were maintained at room temperature and 300 rpm, respectively,

the amount of potassium chloride (0.033 M) was fixed as 0.1 mL.

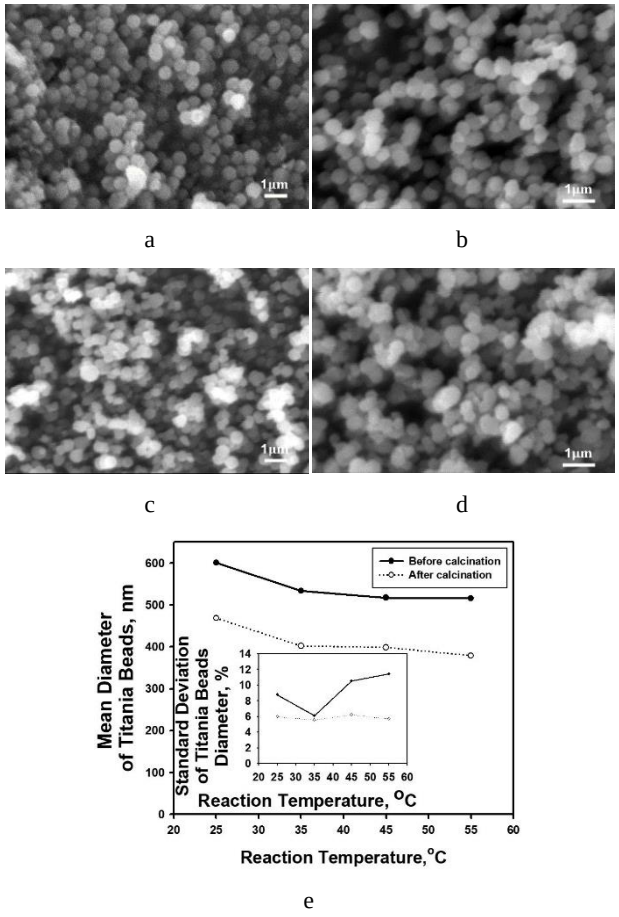

Fig. 8. SEM image of titania beads before calcination synthesized using 0.042 g HDA, 0.1 mL TIP, 0.1 mL KCl (0.033M) at: a – 25 °C; b – 35 °C; c – 45 °C; d – 55 °C; e – change of mean diameter and standard deviation of titania beads before and after calcination as a function of reaction temperature. The rotation speed of the inner cylinder was maintained at 300 rpm

The resulting grain morphologies were spherical as shown in SEM images of Fig. 9 a – c. The amount of TIP increased; the mean diameter of titania beads also increased as displayed in the graph of Fig. 9 d. Because the amount of HDA was not completely reacted, it caused the formation of titania beads with a wide size distribution and a larger standard deviation value. However, after calcination, the excess amount of HDA was removed, so the standard deviation value was smaller as shown in the inner graph of Fig. 9 d.

Secondly, the effect of KCl was investigated by changing the amount of its, while reaction temperature and rotation speed were maintained at room temperature and 300 rpm, the amount of TIP and HDA was fixed as 0.1 mL and 0.042 g, respectively. When the amount of KCl was increased, the diameter of titania beads was reduced, as shown in the SEM image of Fig. 10 a – c, the size distribution in the graph of Fig. 10 d, and the standard deviation value was smaller as shown in the inner graph of Fig. 10 d. KCl was present as an agent used to control the monodispersity of the precursor beads by adjusting the ionic strength of the solution [22]. When the amount of KCl was increased, the monodispersity of the precursor beads was increased, causing the increase of grain number density, and so reducing the size of the titania beads under the same reactant concentrations.

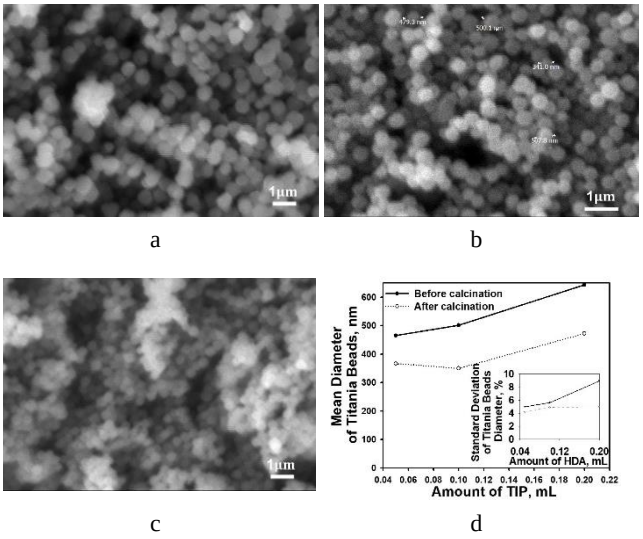

Fig. 9. SEM image of titania beads before calcination synthesized using 0.1 mL KCl (0.033 M): a – 0.084 g HDA, 0.2 mL TIP; b – 0.042 g HDA, 0.1 mL TIP; c – 0.021 g HDA, 0.05 mL TIP; d – change of mean diameter and standard deviation of titania beads before and after calcination as a function of the amount of TIP and HDA at room temperature. The rotating speed of the inner cylinder system was maintained at 300 rpm

FT-IR spectroscopy is a valuable tool for understanding the role of HDA in the formation of titania beads before calcination shown in Fig. 11 a. The first strong difference starting from wavenumbers is the strong reduction of some peaks around 2919, 2850, 1467, 1057 cm^{-1}. FT-IR spectrum shows at 2919 cm^{-1} asymmetrical stretching, and at 2850 cm^{-1} symmetrical stretching of C-H_2 [28, 29]. The peak at 1467 cm^{-1} corresponds to N-H_2 scissoring [27]. The peak at 1057 cm^{-1} corresponds to C-N stretching. Finally, the sharp peak at 723 cm^{-1} appears, belonging to C-H_2 rocking along the carbon chain. In conclusion, the FTIR spectroscopy measurements clearly show the disappearance of HDA in the titania bead after calcination.

X-ray diffraction (XRD) analysis was used to determine the crystal structure of the titania beads and the results are presented in Fig. 11 b. XRD patterns of titania beads before and after calcination at 500 °C for 5 hours were measured in the range of 2θ from 10 to 80°. Titania beads before calcination the diffraction peaks do not appear clearly, and the peaks of titania beads after calcination indicated a mixed phase of anatase and rutile TiO_2. Titania beads were obtained after calcination consisted of primary anatase and small rutile phases corresponding to 25.38° and 27.40° of XRD peaks, respectively [30]. The characteristic peaks at 25.38, 38.10, 48.15, and 54.02° could be assigned as (101), (0.04), (200), and (105) reflection planes of anatase TiO_2 [31]. Though non-crystalline grains were observed after synthesis in a rotating cylinder system, anatase and rutile titania could be produced after calcination, implying that heat treatment caused the transformation from amorphous to crystalline titania grains.

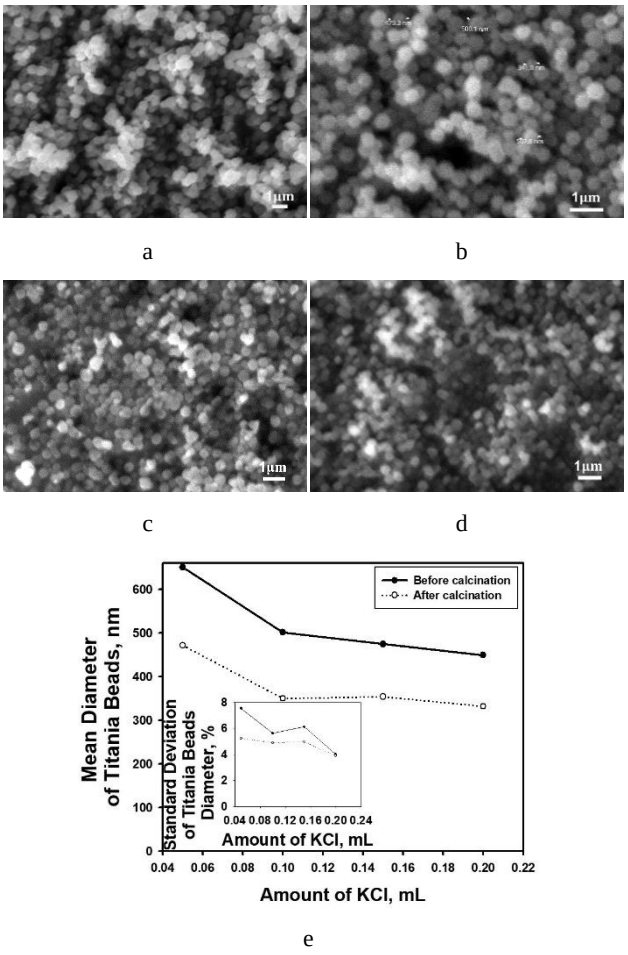

Fig. 10. SEM image of titania beads before calcination synthesized using 0.1 mL TIP, 0.042 g HDA: a – 0.05 mL KCl; b – 0.1 mL KCl; c – 0.15 mL KCl; d – 0.2 mL KCl; e – change of mean diameter and standard deviation of titania beads before and after calcination as a function of the amount of KCl at room temperature. The rotating speed of the inner cylinder system was maintained at 300 rpm

Fig. 12 presents the photocatalytic degradation results of methylene blue using a slurry-type batch photocatalytic reactor containing titania beads under UV-light irradiation. In Fig. 12 a, the kinetics of the decomposition reaction is illustrated by plotting C/C_0 versus degradation time. Accordingly, the results of the plots show that the photodegradation process takes place gradually over the irradiation time. For comparison, three samples of titania beads were carried out to perform photocatalysts. The results showed that titania beads were possible to use for the removal of the organic dye, the degradation rate of titania beads fabricated by the Taylor Vortex reactor was faster than titania beads produced by a round bottom flask, and the removal efficiency was about 63 % for 240 min UV Irradiation. The removal efficiency of titania beads fabricated by a round bottom flask was about 32 %. From here, it shows the rotating cylinder system's ability to synthesize titania beads with a good photocatalytic effect. The removal efficiency of titania beads produced by a round bottom flask when not heat-treated was only about 4.5 %, implying that high-temperature calcination might cause phase transformation of the titania beads, resulting in enhancement of active radical generation from the titania surface for photoreaction in the photocatalytic reactor.

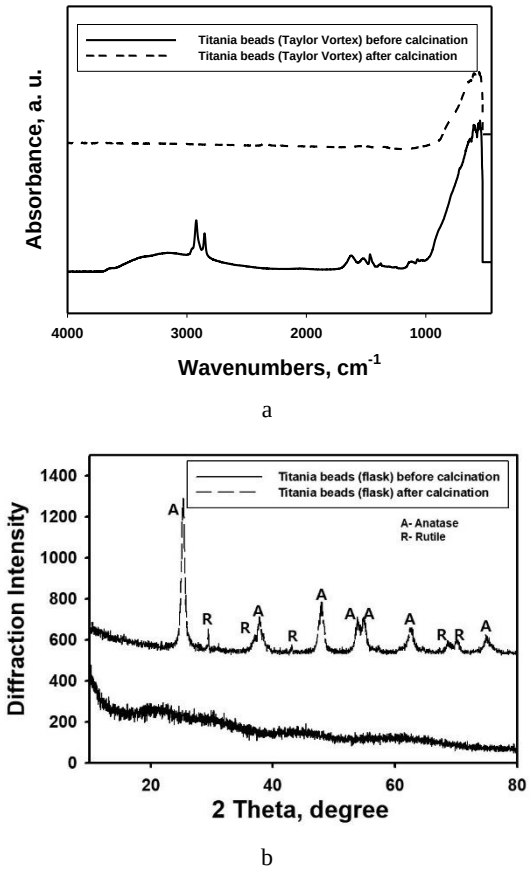

Fig. 11. a – FT-IR spectra of titania beads synthesized using a rotating cylinder system before and after calcination; b – powder XRD results of titania beads synthesized using a round bottom flask before and after calcination

From the semi-log plot of Fig. 12 b, the rate constant of the decomposition reaction could be estimated assuming first-order kinetics of transient concentration, $C(t) = C_0 e^{-kt}$. The linear form of the first-order kinetic model can be stated by the following equation:

$$-ln(C/C_0) = kt, \quad (1)$$

where k denotes the rate constant of the degradation reaction (min^{-1}); C_0 and C are the initial concentration of methylene blue and the concentration of methylene blue (g/mL) at time t, respectively. From Fig. 12 b, the rate constant (k values) using titania beads fabricated by round bottom flask before calcination, titania beads fabricated by round bottom flask after calcination, and titania beads fabricated by Taylor Vortex after calcination could be estimated as 0.000173, 0.001475, and 0.004114 min^{-1}, respectively, by linear regression. After calcination, the photocatalytic ability of titania beads (flask) after calcination is better than titania beads (flask) before calcination, which shows the effect of heat treatment on titania beads. Furthermore, the degradation rate of titania beads synthesized from the Taylor Vortex reactor was faster than that of titania beads synthesized from the round bottom flask. From this, it can be concluded that Taylor Vortex's shaft rotation mechanism can produce titania beads with smaller sizes and better dispersibility.

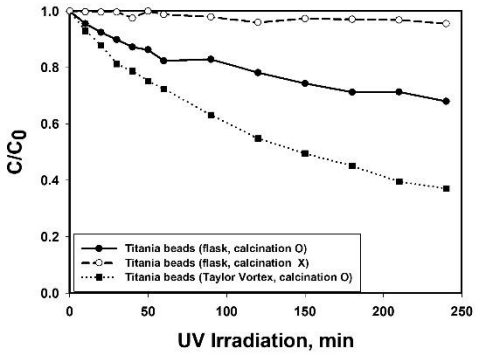

a

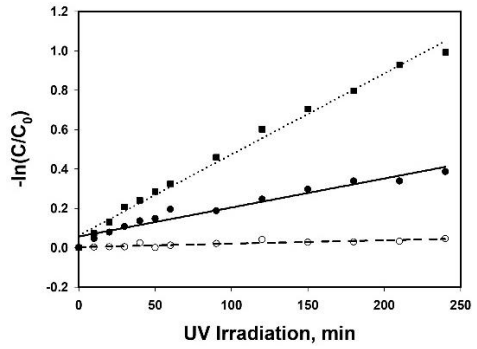

b

Fig. 12. a – change of methylene blue concentration (C/C_0) as a function of UV irradiation time by photocatalytic degradation using titania beads fabricated by round bottom flask and Taylor vortex reactor; b – rate constant of photocatalytic decomposition reaction estimated from data of methylene blue concentration as a function of UV irradiation time using titania beads fabricated by round bottom flask and Taylor Vortex reactor

4. CONCLUSIONS

Silica nanospheres with narrow size distribution were synthesized by rotating cylinder system using low-grade reaction medium and silica precursor. The reaction temperature and rotating speed of the inner cylinder were adjusted for control the mean diameter of grains and size distribution. Reactant compositions such as concentration of precursor and ammonia catalyst were also changed to control the grain size. By successive addition of precursor during reaction, the grain diameter could be adjusted from about 616 to 770 nm. In addition to silica nanospheres, titania beads were also synthesized from the rotating cylinder system. The size distribution of the titania beads was controlled by adjusting reaction temperature, rotation speed and the amount of KCl or titania precursor, TIP. Titania beads were fabricated by a Taylor Vortex reactor, which could better remove the organic dye in an aqueous medium using a photocatalytic decomposition system than titania beads were fabricated by a round bottom flask. These could provide useful information about the photolysis of organic dyes for water purification, recycling technology, and other fields.

Acknowledgments

This research was supported by Priority Research Centers Program through the National Research Foundation of Korea (NRF) funded by the Ministry of Education (NRF-2017R1A6A1A03015562) and Korea Institute for Advancement of Technology (KIAT) grant funded by the Korea Government (MOITIE, P0002007, The Competency Development Program for Industry Specialist).

REFERENCES

1. **Zhu, C., Chen, L., Xu, H., Gu, Z.** A Magnetically Tunable Colloidal Crystal Film for Reflective Display *Macromolecular Rapid Communications* 30 (22) 2009: pp. 1945 – 1949. https://doi.org/10.1002/marc.200900392
2. **Elsanousi, A., Taha, K.K., Elamin, N.** Synthesis of Porous Titania and Its Application to Dye-Sensitized Solar Cells *Advanced Materials Letters* 4 (12) 2013: pp. 905 – 909. https://doi.org/10.5185/amlett.2013.5472
3. **Dutt, A.K., Datta, A.** Imperfect Mixing and Dead-Zone Effects in Nonlinear Dynamics: Law of Mass Action Revisited *The Journal of Physical Chemistry A* 102 (41) 1998: pp. 7981 – 7983. https://doi.org/10.1021/jp982629i
4. **Racina, A., Liu, Z., Kind, M.** Mixing in Taylor-Couette Flow. Micro and Macro Mixing. Heat and Mass Transfer. Springer, Berlin, Heidelberg. 2010: pp.125 – 139. https://doi.org/10.1007/978-3-642-04549-3_8
5. **Wang, L.** Computational fluid dynamics simulation of precipitation processes. Retrospective Theses and Dissertations, Paper 1202, 2004. https://doi.org/10.31274/rtd-180813-10902
6. **Sprague, M.A., Weidman, P.D., Macumber, S., Fischer, P.F.** Tailored Taylor Vortices *Physics of Fluids* 20 (1) 2008: pp. 014102. http://doi.org/10.1063/1.2831493
7. **Ogihara, T., Matsuda, G., Yanagawa, T., Ogata, N., Fujita, K., Nomura, M.** Continuous Synthesis of Monodispersed Silica Particles Using Couette-Taylor Vortex Flow *Journal of the Ceramic Society of Japan* 103 (2) 1995: pp. 151 – 154. http://doi.org/10.2109/JCERSJ.103.151
8. **Yamamoto, T., Itoh, K., Maeda, K., Fukui, K., Kuramochi, H.** Effect of Taylor Vortex on Melt Crystallization of Fatty Acids *Crystal Research and Technology* 54 (7) 2019: pp. 1900050. http://doi.org/10.1002/crat.201900050
9. **Nam, K.H., Kim, U.J., Jeon, M.H., Lee, T.R., Yu, J., You, N.H., Kim, Y.K., Suk, J.W., Ku, B.C.** Green, Fast, and Scalable Production of Reduced Graphene Oxide Via Taylor Vortex Flow *Chemical Engineering Journal* 391 2020: pp. 123482. http://doi.org/10.1016/j.cej.2019.123482
10. **Heo, K., Lee, J., Song, Y.W, Kim, M.Y., Jeong, H., Cheon, A.D., Kim, J., Lim, J.** Synthesis and Electrochemical Performance Analysis of $LiNiO_2$ Cathode Material Using Taylor-Couette Flow-Type Co-Precipitation Method *Journal of The Electrochemical Society* 168 (1) 2021: pp. 010521. http://doi.org/10.1149/1945-7111/abd91a
11. **Wang, B., Tao, S.** Synthesis of Micro-/Nanohydroxyapatite Assisted by the Taylor−Couette Flow Reactor *ACS Omega* 7 (48) 2022: pp. 44057 – 44064. https://doi.org/10.1021/acsomega.2c05491
12. **Lee, B.K., Jung, Y.H., Kim, D.K.** Synthesis of Monodisperse Spherical SiO_2 and Self-Assembly for

Photonic Crystals *Journal of the Korean Ceramic Society* 46 (5) 2009: pp. 472 – 477. https://doi.org/10.4191/KCERS.2009.46.5.472

13. **Cong, H., Yu, B., Wang, S., Qi, L., Wang, J., Ma, Y.** Preparation of Iridescent Colloidal Crystal Coatings with Variable Structural Colors *Optics Express* 21 (15) 2013: pp. 17831 – 17838. http://doi.org/10.1364/OE.21.017831
14. **Holtz, J.H., Holtz, J.S.W., Munro, C.H., Asher, S.A.** Intelligent Polymerized Crystalline Colloidal Arrays: Novel Chemical Sensor Materials *Analytical Chemistry* 70 (4) 1998: pp. 780 – 791. https://doi.org/10.1021/ac970853i
15. **Li, G., Xiao, F., Li, S., Chen, Q., Zhou, J., Wu, Z., Yu, R.** Label-free 2D Colloidal Photonic Crystal Hydrogel Biosensor for Urea and Urease Inhibitor *Sensors and Actuators B: Chemical* 277 (20) 2018: pp. 591 – 597. http://doi.org/10.1016/j.snb.2018.09.059
16. **Cho, Y.S., Shin, C.H.** Synthesis of Monodisperse Silica Particles using Rotating Cylinder Systems *The Korean Institute of Chemical Engineers* 54 (6) 2016: pp. 792 – 799. https://doi.org/10.9713/kcer.2016.54.6.792
17. **Wang, X., Cao, L., Chenm, D., Caruso, R.A.** Engineering of Monodisperse Mesoporous Titania Beads for Photocatalytic Applications *ACS Applied Materials & Interfaces* 5 (19) 2013: pp. 9421 – 9428. https://doi.org/10.1021/am401867s
18. **Ovenstone, J., Yanagisawa, K.** Effect of Hydrothermal Treatment of Amorphous Titania on the Phase Change from Anatase to Rutile during Calcination *Chemistry of Materials* 11 (10) 1999: pp. 2770 – 2774. https://doi.org/10.1021/cm990172z
19. **Huang, Y., Wu, H., Yu, Q., Wang, J., Yu, C., Wang, J., Gao, S., Jiao, S., Zhang, X., Wang, P.** Single-Layer TiO_2 Film Composed of Mesoporous Spheres for High-Efficiency and Stable Dye-Sensitized Solar Cells *ACS Sustainable Chemistry & Engineering* 6 (3) 2018: pp. 3411 – 3418. https://doi.org/10.1021/acssuschemeng.7b03626
20. **Xichao, Z., Wen-Fan, C., Ghazaleh, B., Vishesh, K., Naomi, H., Pramod, K., Charles, C.S.** Synthesis of V-and Mo-doped/codoped TiO_2 Powders for Photocatalytic Degradation of Methylene Blue *Nano-Structures & Nano-Objects* 24 2020: pp.100557. http://doi.org/10.1016/j.nanoso.2020.100557
21. **Vishesh, K., Wen-Fan, C., Xichao, Z., Yue, J., Pramod, K., Charles, C.S.** Properties and Performance of Photocatalytic CeO_2, TiO_2, and CeO_2-TiO_2 Layered Thin Films *Ceramics International* 45 2019: pp. 22085 – 22094. http://doi.org/10.1016/j.ceramint.2019.07.225
22. **Chen, D., Cao, L., Huang, F., Imperia, P., Cheng, Y.B., Caruso, R.A.** Synthesis of Modisperse Mesoporous Titania Beads with Controllable Diameter, High Surface Areas, and Variable Pore Diameters (14 – 23 nm) *Journal of the American Chemical Society* 132 (12) 2010: pp. 4438 – 4444. https://doi.org/10.1021/ja100040p
23. **Cho, Y.S, Hwang, C, Kim, S.J., Park, U.H.** Continuous Synthesis of Monodisperse Spherical Silica Powder Using Tubular Reaction System *The Korean Journal of Metals and Materials* 60 (6) 2022: pp. 409 – 422. http://doi.org/10.3365/KJMM.2022.60.6.409
24. **Krzysko, A.J., Nakouzi, E., Zhang, X., Graham, T.R., Rosso, K.M., Schenter, G.K., Ilavsky, J., Kuzmenko, I., Frith, M.G., Ivory, C.F., Clark, S.B., Weston, J.S., Weigandt, K.M., DeYoreo, J.J., Chun, J., Anovitz, L.M.** Correlating Inter-Particle Forces and Particle Shape to Shear-Induced Aggregation/Fragmentation and Rheology for Dilute Anisotropic Particle Suspensions: A Complementary Study via Capillary Rheometry and in Situ Small and Ultra-Small Angle X-Ray Scattering *Journal of Colloid and Interface Science* 576 2020: pp. 47 – 58. https://doi.org/10.1016/j.jcis.2020.04.016
25. **Koganti, V.R., Das. S., Rankin, S.E.** In Situ FTIR Investigation of the Kinetics of Silica Polycondensation in Surfactant Templated, Mesostructured Thin Films *The Journal of Physical Chemistry C* 118 (33) 2014: pp. 19450 – 19461. http://doi.org/10.1021/jp505651j
26. **Waseem, M., Mustafa, S., Naeem, A., Shah, K.H., Shah, I., Haque, I.** Synthesis and Characterization of Silica by Sol-Gel Method *Journal of the Pakistan Materials Society* 3 (1) 2009: pp. 19 – 21.
27. **Dubey, R.S., Rajesh, Y.B.R.D., More, M.A.** Synthesis and Characterization of SiO_2 Nanoparticles via Sol-Gel Method for Industrial Applications *Materials Today: Proceedings* 2 (4 – 5) 2015: pp. 3575 – 3579. https://doi.org/10.1016/j.matpr.2015.07.098
28. **Mallikarjuna, K., Deva Prasad Raju, B., Sumi Park, S., Kim, H.** Synthesis and Catalytic Activity of Alkylamine-Capped Ultra-small Palladium Nanoparticles for Organic Pollutant Degradation *Journal of Cluster Science* 28 (5) 2017: pp. 2833 – 2846. http://doi.org/ 10.1007/s10876-017-1262-5
29. **Eck, M.** Performance Enhancement of Hybrid Nanocrystal/Polymer Bulk Heterojunction Solar Cells: Aspects of Device Efficiency, Reproducibility, And Stability. Breisgau: Abert-Ludwigs-Universität Freiburg, 2014.
30. **Chang, M.C.** Nitrogen Doping in Polycrystalline Anatase TiO_2 Ceramics by Atmosphere Controlled Firing *Journal of the Korean Ceramic Society* 56 (4) 2019: pp. 374 – 386. https://doi.org/10.4191/kcers.2019.56.4.07
31. **Li, X., Zhang, Z., Zhang, F.J., Liu, J., Ye, J., Oh, W.C.** Synthesis and Photocatalytic Activity of TiO_2/$BiVO_4$ Layered Films under Visible Light Irradiation *Journal of the Korean Ceramic Society* 53 (6) 2016: pp. 665 – 669. https://doi.org/10.4191/kcers.2016.53.6.665